Nonlinear Modeling and Design of Initial Position Estimation and Polarity Detection of IPM Drives

Yingguang Sun, *Student Member, IEEE,* Matthias Preindl, *Member, IEEE,*
Shahin Sirouspour, *Member, IEEE,* and Ali Emadi, *Fellow, IEEE*
Department of Electrical and Computer Engineering,
McMaster University, Hamilton, Ontario, Canada
Email: suny77@mcmaster.ca, preindl@mcmaster.ca, sirous@mcmaster.ca, emadi@mcmaster.ca

***Abstract*—This paper proposes a novel initial rotor position estimation algorithm for Interior Permanent Magnet Synchronous Machine (IPMSM) drives. First, the rotor position is determined based on the machine saliency using the flux equations in the stationary reference frame. Since the machine saliency performs two periods in one electrical cycle, there exists an ambiguity of 180° in the estimation result. The location of the magnetic north pole is detected using a generalized polarity detection method. This method injects voltage pulses and compares the current response with the expected response using the d-axis differential inductance profile. An accurate nonlinear machine model is introduced for analysis and simulation of sensorless control in IPMSM drives. The model uses the machine flux as dynamic equation and the flux current relationship as output function avoiding approximations due to saturation. The initial position detection procedure is validated with this model using experimental current-flux data.**

I. Introduction

Permanent magnet synchronous machines are known for their fast response, high efficiency, high power density and ease of control. However, synchronous machines require the rotor position and speed information for control. The position sensors which are normally used in the PM machines have several disadvantages such as reduced reliability, increased size, additional cost and increased complexity of the drive system [1]. Consequently, researchers have been investigating new methods for position and speed sensorless control of IPMSM drives to avoid sensor-related issues [2]–[9].

Machine models are instrumental in the analysis of the performance and tuning of the parameters of position estimation algorithms prior to actual experimental validation. The typical machine model assumes constant parameters and is widely used for such purposes. However, this machine model is not suitable for position estimation especially for polarity detection, because of their inaccuracies and their inability to model nonlinearities, which some of these methods rely on. Look-up tables relating current to inductance or flux linkage are commonly employed for nonlinear machine modeling. The use of the derivative of flux in the machine dynamics often gives rise to oscillations and can reduce the accuracy of transient response, when using look-up table based models. An improved method for implementing the nonlinear machine model is introduced in this paper and is used for investigating the performance of the initial position estimation algorithm.

In position sensorless control, the rotor position must be estimated in the rotating state as well as standstill condition, especially at the machine startup. Several methods have been introduced [7], [9]–[12]. In [7], the current components for estimating the initial position are difficult to obtain and are affected by significant measurement noise. The methods proposed in [10], [11] have complex injection procedure and criterion for determining initial position. In [9], [11], [12], the saturation effect of the stator core is used, which requires high currents that can be significantly above the rated current.

This paper proposes a new method for initial position estimation. In this method, a short rectangular voltage pulse is injected in the stationary reference frame and the peak value of the position-dependent current response is used for calculating the initial rotor position. The main advantage of this method is its simplicity and ease of implementation compared to other existing techniques in the literature. Given that the proposed approach exploits the machine saliency, it can only determine the initial rotor position with an ambiguity of 180°, as the machine saliency performs two periods in one electrical cycle.

In [9]–[12], the magnetic saturation of the stator core was used to determine the location of the north magnetic pole. However, the current needed to saturate the stator core is usually much higher than the rated current of the machine, requiring inverters with higher power rating to ensure robust detection of magnetic polarity. This paper presents a generalized approach to polarity detection that exploits asymmetries in machine specific differential inductance-current profile in d-axis. This approach can lead to more robust estimation of the polarity that is less sensitive to measurement noise and can operate with smaller injected currents.

In summary, the contributions of this paper are: (i) an enhanced method for implementation of nonlinear IPMSM model (ii) a simple algorithm for estimation of initial rotor position and (iii) a generalized polarity detection method using IPMSM flux linkage profile. The rest of the paper is organized as follows. Section II introduces the implementation method for nonlinear motor model. Section III presents the new strategy for the initial rotor position estimation. Section IV is concerned with the generalized polarity detection algorithm. In Section V, results of simulations of the combined initial position estimation method based on the nonlinear machine model are presented. The paper is concluded in Section VI.

978-1-4799-1762-4/15/$31.00 ©2015 IEEE 004059

II. Nonlinear Machine Modeling

Typical machine model with constant L_d and L_q values was widely used in simulation analysis of the machine drive system. This model is based on the dynamic equations in d-q frame i.e.,

$$u_d = Ri_d + L_d\frac{di_d}{dt} - \omega_e L_q i_q \qquad (1)$$
$$u_q = Ri_q + L_q\frac{di_q}{dt} + \omega_e L_d i_d + \omega_e \lambda_{pm}$$

where u_{dq}, i_{dq} and L_{dq} denote the voltages and currents in d-q frame. R, ω_e and λ_{pm} represent the phase resistance, electrical speed and permanent magnet flux linkage respectively.

Besides the above machine modeling, nonlinear machine model with flux linkage or inductance profiles are also used. These profiles are either obtained from finite element analysis software or from experiment results. These profiles are implemented as look-up tables (LUTs) in the nonlinear machine model. Dynamic equations of the nonlinear machine model can be rewritten as,

$$u_d = Ri_d + \frac{d\lambda_d(i_d,i_q)}{dt} - \omega_e\lambda_q(i_d,i_q) \qquad (2)$$
$$u_q = Ri_q + \frac{d\lambda_q(i_d,i_q)}{dt} + \omega_e\lambda_d(i_d,i_q)$$

where $\lambda_d(i_d,i_q)$ and $\lambda_q(i_d,i_q)$ represent the flux linkage profiles in d-q frame.

As evident from the above equations, the derivatives of the flux linkage profiles are needed in the implementation of the machine model which can introduce oscillations in the transients. If these profiles can be inverted to current profiles $i_d(\lambda_d,\lambda_q)$ and $i_q(\lambda_d,\lambda_q)$, only integration would be need in the implementation of the dynamics, hence avoiding numerical issues related to taking numerical derivatives. However, these inverse LUTs can not be obtained directly from experiment because currents are commonly applied in the motor drive system instead of flux. In order to solve this problem, a novel way of inverting look-up tables has been proposed in this paper. Fig. 1 shows the flowchart of the proposed look-up table inversion algorithm, which involves the following steps:

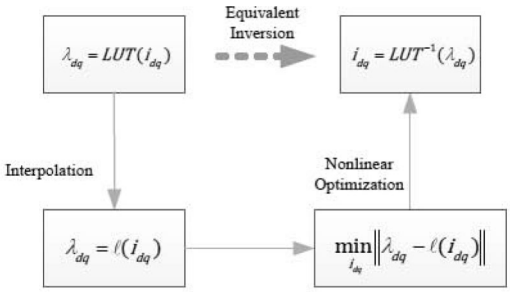

Fig. 1. Flowchart of look-up table inversion algorithm

1) The functions λ_{dq}=$\ell(i_{dq})$ can be obtained by interpolating the original look-up tables.
2) The obtained functions are used in calculating the inverse look-up tables. The inversion is a least squares problem which can be solved with nonlinear numerical solvers.
3) The returned current values together with the input flux linkage values are recorded in the form of look-up tables.

By following the above procedures, the inverse look-up tables $i_{dq} = LUT^{-1}(\lambda_{dq})$ can be achieved and Fig. 2 shows the original and inverse LUTs derived from experimental data from an actual machine used in this paper.. All the flux linkage and current values are given in per unit value.

Fig. 3 depicts the block diagram of the nonlinear machine model dynamics. The dynamic equations now can be rewritten in the discrete form,

$$\begin{bmatrix} \lambda_d(n+1) \\ \lambda_q(n+1) \end{bmatrix} = \begin{bmatrix} 1 & T_s\omega_e(n) \\ -T_s\omega_e(n) & 1 \end{bmatrix} \begin{bmatrix} \lambda_d(n) \\ \lambda_q(n) \end{bmatrix} \qquad (3)$$
$$+ T_s \begin{bmatrix} u_d(n) \\ u_q(n) \end{bmatrix} - T_s R \begin{bmatrix} i_d(n) \\ i_q(n) \end{bmatrix}$$

where $\lambda_{dq}(n+1)$ denotes the d and q axis flux linkage in current sample time. $\lambda_{dq}(n)$, $u_{dq}(n)$, $i_{dq}(n)$ and $\omega_e(n)$ represent the flux linkage, voltage, current and electrical speed in the previous sample time. T_s represents the sampling time. The $A(\omega_e)$ matrix in Fig. 3 is $A(\omega_e) = (I - \omega_e(n)T_sJ)$, where I is the identity matrix and $J = \begin{bmatrix} 0 & -1 \\ 1 & 0 \end{bmatrix}$. The dynamic equations in (3) avoid numerical differentiation of the flux values and hence have improved numerical behavior.

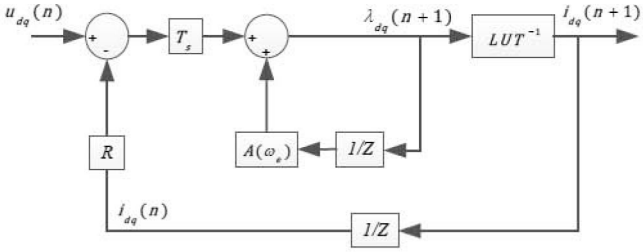

Fig. 3. Block diagram of the nonlinear machine model dynamics with inverse LUTs

III. Initial Rotor Position Estimation

The stationary reference frame (α-β frame) refers to the frame which is stationary with respect to the stator windings. The three phase voltages and currents are transformed into α-β frame by using

$$\begin{bmatrix} f_\alpha \\ f_\beta \end{bmatrix} = \frac{2}{3}\begin{bmatrix} 1 & -\frac{1}{2} & -\frac{1}{2} \\ 0 & \frac{\sqrt{3}}{2} & -\frac{\sqrt{3}}{2} \end{bmatrix} \begin{bmatrix} f_a \\ f_b \\ f_c \end{bmatrix}, \qquad (4)$$

where $f_{\alpha\beta}$ and f_{abc} denote the voltages and currents in α-β frame and a-b-c frame respectively.

Assuming that the motor shaft does not move as a result of injecting short rectangular voltage pulses in α axis for one sample time T_s and the phase resistance is compensated [13], the corresponding equations (5) and (6) can be shown as following:

$$\theta(T_s) = \theta(0) \qquad (5)$$

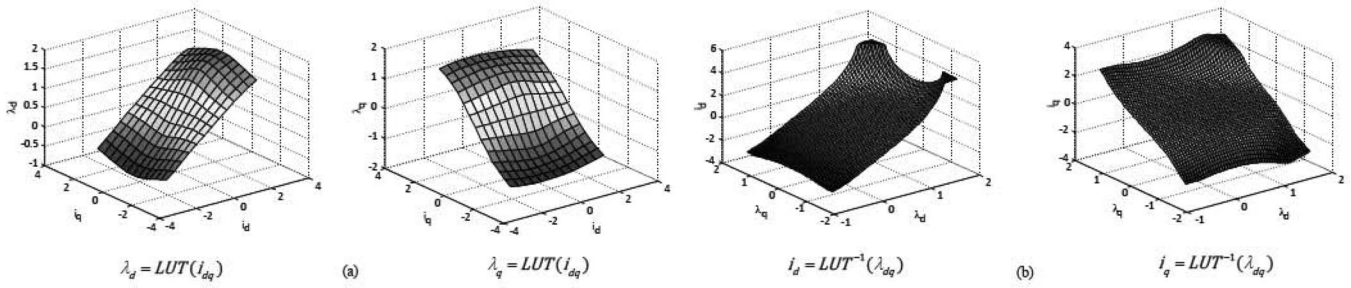

Fig. 2. Look-up tables. (a) Original look-up tables. (b) Inverse look-up tables

$$\begin{bmatrix} \lambda_\alpha(0) \\ \lambda_\beta(0) \end{bmatrix} = \lambda_{pm} \begin{bmatrix} \cos\theta(0) \\ \sin\theta(0) \end{bmatrix} \tag{6}$$

where $\theta(0)$ and $\theta(T_s)$ denote the rotor position before and after injection respectively. $\lambda_\alpha(0)$ and $\lambda_\beta(0)$ represent the initial flux linkage in α-β frame.

Based on the above assumptions, the flux linkage equations in α-β frame can be obtained both from the injected voltages and induced currents:

$$\begin{bmatrix} \lambda_\alpha(T_s) \\ \lambda_\beta(T_s) \end{bmatrix} = \begin{bmatrix} \lambda_\alpha(0) \\ \lambda_\beta(0) \end{bmatrix} + T_s \begin{bmatrix} \bar{u}_\alpha(0) \\ \bar{u}_\beta(0) \end{bmatrix}, \tag{7}$$

$$\begin{bmatrix} \lambda_\alpha(T_s) \\ \lambda_\beta(T_s) \end{bmatrix} = \lambda_{pm} \begin{bmatrix} \cos\theta(0) \\ \sin\theta(0) \end{bmatrix} + \begin{bmatrix} \frac{L_2}{2} + \frac{L_1}{2}\cos 2\theta(T_s) & \frac{L_1}{2}\sin 2\theta(T_s) \\ \frac{L_1}{2}\sin 2\theta(T_s) & \frac{L_2}{2} - \frac{L_1}{2}\cos 2\theta(T_s) \end{bmatrix} \begin{bmatrix} i_\alpha(T_s) \\ i_\beta(T_s) \end{bmatrix}, \tag{8}$$

where $L_1 = L_d - L_q$ and $L_2 = L_d + L_q$. $\lambda_{\alpha\beta}$, $i_{\alpha\beta}$ and $\bar{u}_{\alpha\beta}$ denote the flux linkages, currents and compensated voltages in α-β frame respectively. To be specific, $\bar{u}_{\alpha\beta} = u_{\alpha\beta} - Ri_{\alpha\beta}$, where R represents the phase resistance and $u_{\alpha\beta}$ denotes uncompensated voltage in α-β frame.

Combining (5), (6), (7) and (8) yields the following equation

$$\begin{bmatrix} \frac{L_2}{2} + \frac{L_1}{2}\cos 2\theta(0) & \frac{L_1}{2}\sin 2\theta(0) \\ \frac{L_1}{2}\sin 2\theta(0) & \frac{L_2}{2} - \frac{L_1}{2}\cos 2\theta(0) \end{bmatrix} \begin{bmatrix} i_\alpha(T_s) \\ i_\beta(T_s) \end{bmatrix} - T_s \begin{bmatrix} \bar{u}_\alpha(0) \\ \bar{u}_\beta(0) \end{bmatrix} = 0. \tag{9}$$

Note that these equations only involve the voltage and current values, which are usually measured in IPMSM drives, and the unknown initial rotor position.

The injected voltage in α axis is two thirds of the DC link voltage and the injection duration is one sampling time T_s. The stationary reference frame injection technique is implemented as following:

1) The gate signals for phase A, B and C are controlled to generate voltage pulse in α axis. The voltage vector V(100) is applied for T_s and then the vector V(011) is applied to force the currents decrease to zero, as shown in Fig. 4.
2) The peak values of the current responses in α-β frame are recorded.
3) The recorded peak current values and the applied voltages are used in solving the nonlinear equation (9).

Fig. 5 shows the equivalent injection voltage and current responses in α-β frame. The controller sampling time is 100 μs. So the peak current values in the red circles can be recorded. Combined with the injected voltage in α axis, the estimated initial rotor position can be calculated by (9).

The initial rotor position $\theta(0)$ can be obtained as the solution to a nonlinear least-squares optimization based on (9), which can be easily solved using line search approaches [14].

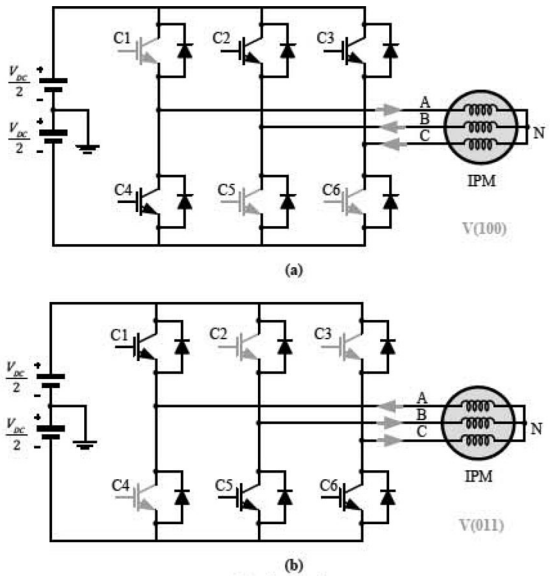

Fig. 4. Voltage vectors applied for injection. (a) V(100). (b) V(011).

IV. Magnetic Polarity Detection

In section III, the solution to (9) would have an ambiguity of 180° because all the entries in the inductance matrix contain $2\theta(0)$ instead of $\theta(0)$.

Existing magnetic polarity detection methods [9], [11], [12] utilize the magnetic saturation effect of the stator core. The flux linkage in d axis saturates under positive current. In [9], [12], a dual voltage pulses are injected. The pulse aligned with the north pole increases the magnetization of the stator core and leads to a lower L_d. The peak value of the induced current by this pulse is larger. The other pulse aligned with the south pole decreases the magnetization of the stator core and results in a higher L_d. The peak value of the induced current by this

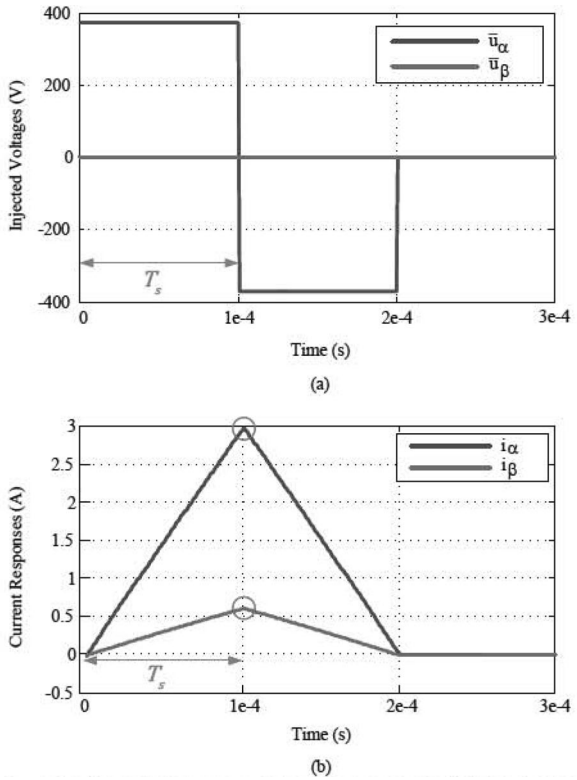

Fig. 5. Injection voltages and current responses in α-β frame. (a) Injection voltage in α-β frame. (b) Current responses in α-β frame.

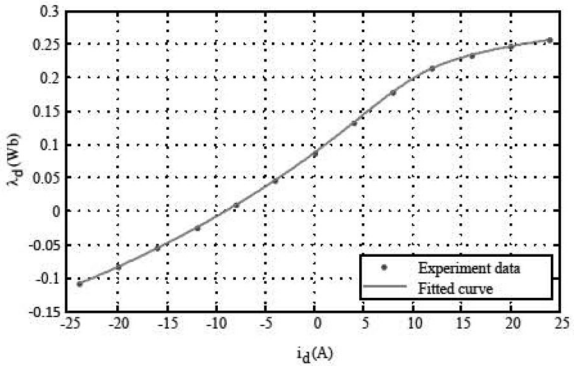

Fig. 6. λ_d versus i_d for i_q= 0

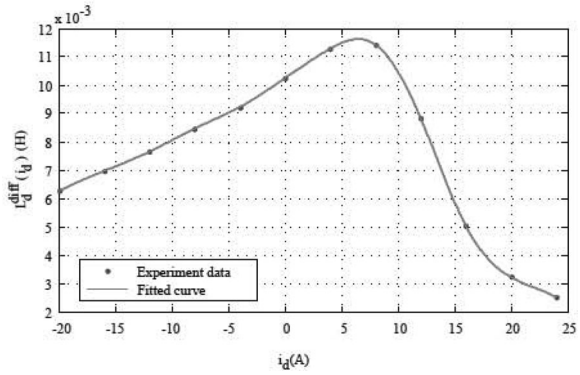

Fig. 7. $L_d^{diff}(i_d) = \frac{d\lambda_d}{di_d}$ versus i_d for i_q= 0

pulse is smaller. Since this inductance variation can also be reflected in the phase inductance, so the magnetic polarity can be detected by observing the phase currents as well [11].

However, as mentioned in Section I, the current needed for saturation can be much higher than the rated current of the machine and requires a high power rating power inverter. Moreover, since the flux linkage or inductance profiles are distinct for different machines with specific geometry or design, checking two or three current peak values is not robust in detecting the polarity. In this paper, in order to detect the magnetic polarity, the profiles of λ_d-i_d and L_d^{diff}-i_d for i_q= 0 are utilized, which are shown in Fig. 6 and Fig. 7. The differential inductance L_d^{diff} is defined as $L_d^{diff} = d\lambda_d/di_d$. These profiles can be obtained from finite element analysis software as well as experiments. For flux linkage profiles in this paper, all the data in the profiles comes from the experiments.

The λ_d-i_d curve and L_d^{diff}-i_d curve in Fig. 6 and Fig. 7 can be obtained by fitting the relevant data from experiments. In order to get the measured L_d^{diff}, rectangular voltage pulses are injected in estimated d axis and L_d^{diff} can be approximated by

$$L_d^{diff} = \frac{d\lambda_d}{di_d} = \frac{d\lambda_d}{dt}\frac{dt}{di_d} = \frac{V_{inj}T_s}{\Delta i_d}, \tag{10}$$

where V_{inj} denotes the magnitude of the injected voltage and Δi_d represents the current difference between the current sampling time and previous sampling time. The current $i_d(n)$ can be measured at each sampling time and $L_d^{diff}(n)$ can be calculated by (10) accordingly.

Fig. 8 shows the injected voltage pulses and current responses. Only the current responses of the blue injection voltages are used for polarity detection. The green voltage pulses are used for forcing the current response return to zero. In Fig. 8, each voltage pulse lasts for two sample times and four sets of data $(i_d(n), L_d^{diff}(n)), n = 1 \ldots 4$ are recorded. If the estimated d axis aligns with the north pole, $(i_d(n), L_d^{diff}(n))$ will be on the curve fitted in Fig. 7. If the estimated d axis aligns with the south pole, $(-i_d(n), L_d^{diff}(n))$ will be on the curve.

In general, if each voltage pulse lasts for nT_s, then the difference between the measured points and the points on the curve can be calculated as following:

$$\begin{aligned}
&\Delta_1(i) = L_d^{diff}(i) - \xi(i_d(i)) \qquad i = 1 \ldots n \\
&\Delta_2(i) = L_d^{diff}(i) - \xi(-i_d(i)) \qquad i = 1 \ldots n \\
&c_1 = \left\|\Delta_1(1)^2 + \Delta_1(2)^2 + \ldots + \Delta_1(n)^2\right\| \\
&c_2 = \left\|\Delta_2(1)^2 + \Delta_2(2)^2 + \ldots + \Delta_2(n)^2\right\|
\end{aligned} \tag{11}$$

where $\xi()$ is the fitted curve in Fig. 7.

Fig. 9 shows the framework of the proposed polarity detection algorithm. The cost c_1 and c_2 can be calculated in (11) based on the injected voltages and the respondent currents. If c_1 is smaller than c_2, the positive direction of d axis aligns with the north pole and the estimated position is correct. While if c_1 is larger than c_2, the positive direction of d axis aligns with the south pole and the estimated position has to be added by 180°.

In Fig. 8, injecting each voltage pulse at two sampling time is just an example. Actually, the proposed method provides

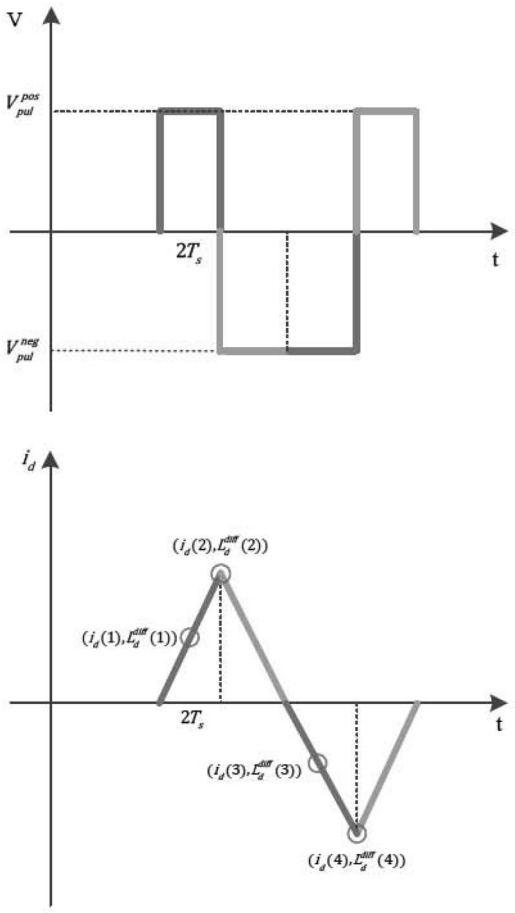

Fig. 8. Injected voltage pulses and current responses in d axis, using n=2 as an example

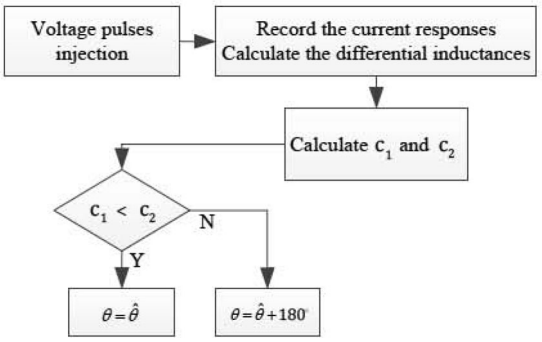

Fig. 9. Framework of the polarity detection

various options for injection voltage magnitude and injection duration. These selections can be made based on the L_d^{diff}-i_d curve. In this way, the optimal injection magnitude and duration can be achieved for different IPM machines.

V. Simulations of Initial Position Estimation Algorithm Based on Nonlinear Machine Model

The proposed initial position estimation approach and polarity detection method are simulated using the proposed implementation of nonlinear machine model discussed in Section II. As shown in Fig. 5, the voltage injected in α-β frame

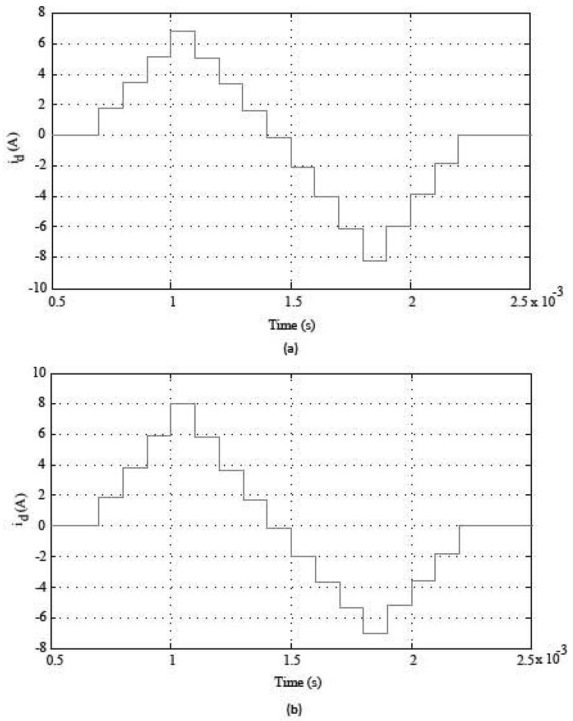

Fig. 10. d axis current responses. (a) d axis current when the estimated rotor position is 60°. (b) d axis current when the estimated rotor position is 300°.

for initial position estimation is 373 V which lasts for one sampling time. For polarity detection, the injection voltage magnitude is 200 V and the injection duration is 400 μs ($4T_s$) for each of the pulses. Fig. 10 shows the d axis current responses of the injection for polarity detection. The current $i_d(n)$ is sampled and recorded for each sampling time. Table I shows the parameters of the IPM machine and drives used in simulation.

TABLE I
Parameters of IPMSM and Drive Used in Simulation [15]

Parameter	Value
Number of pole pairs P	5
Rated current I_r	10 A
Rated torque T_r	8 Nm
Rated flux λ_r	142.5 mWb
d axis inductance L_d	9.1 mH
q axis inductance L_q	14.6 mH
Stator resistance R	636 $m\Omega$
PM flux λ_{pm}	88.3 mWb
Shaft friction B	6.4 $\times 10^{-3}$ Nms
Shaft innertia J	5.0 $\times 10^{-3}$ kgm^2
DC link voltage U_{dc}	560 V
Sampling time T_s	100 μs

The simulation results of the combined initial position estimation and polarity detection algorithms are shown in Fig. 11. At the beginning, one voltage pulse is injected in α axis for T_s to calculate the initial rotor position. Once the position is obtained, voltage pulses shown in Fig. 8 will be injected in the estimated d axis to detect the polarity. If the position obtained from the α axis injection is correct, a compensation of 0° will be added to the estimated position. This condition is shown in Fig. 11(a). If the initial position estimation has an error of 180°, this error will be compensated by the proposed

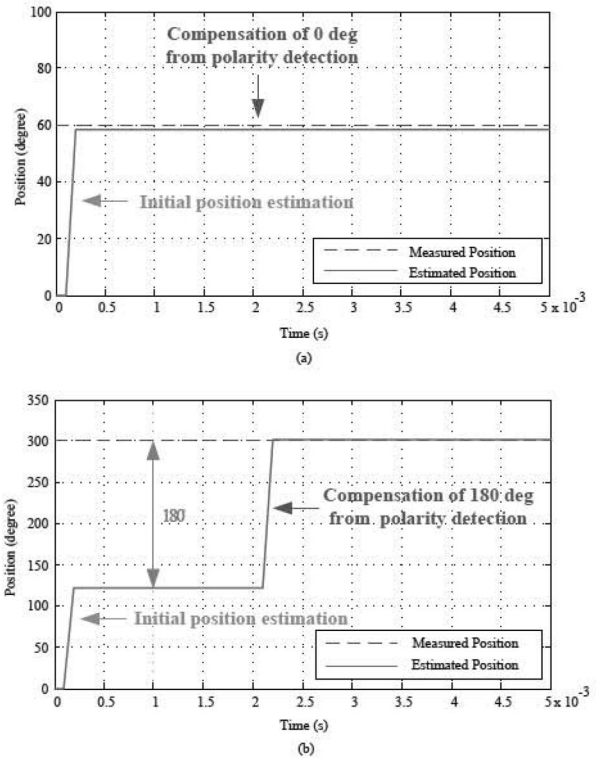

Fig. 11. Position estimation results. (a) Estimation results at 60°. (b) Estimation results at 300°.

polarity detection method, which is shown in Fig. 11(b). In this way, the correct position and polarity estimation can be achieved.

The position estimation results of the combined estimation method are shown in Table II. The position estimation has some uncertainties due to the noises and parameter variations caused by machine non-linearity. Avoiding those uncertainties will be the subject of future research.

TABLE II
POSITION ESTIMATION RESULTS OF THE PROPOSED METHODS

Measured Initial Position (deg)	0°	60°	120°	180°	240°	300°
Estimated Initial Position (deg)	0.2°	58.5°	127.6°	179.9°	232.7°	302.2°
Estimation Error (deg)	0.2°	-1.5°	7.6°	-0.1°	-7.3°	2.2°

VI. CONCLUSION

In this paper, the feasibility of a novel initial position estimation and polarity detection method is investigated and validated with a high fidelity nonlinear machine model with current profiles which are obtained from the inversion of the experimental flux linkage profiles. The current profiles lead to a better implementation of the machine model with high accuracy and better performance in transients.

The proposed initial position estimation algorithm relies on the pulse injection in stationary reference frame and the position can be estimated by solving position-dependent nonlinear equations. This method simplifies the estimation procedures and has the advantage of easy implementation compared with existing methods.

The polarity detection method in this paper generalizes the polarity detection technique for different IPM machines. The polarity can be detected once the differential inductance profile versus current in d axis is known. Compared with methods relying solely on saturation, the proposed method requires significantly lower currents for determining the polarity.

Based on the nonlinear model, the combined initial position and polarity detection method is simulated and investigated. The polarity can be distinguished by applying 70% – 80% of the rated current. For the estimation accuracy, the average estimation error is 3.15° and the maximum estimation error is 7.6°.

ACKNOWLEDGMENT

This research was undertaken, in part, thanks to funding from the Canada Excellence Research Chairs Program.

REFERENCES

[1] A. Emadi, *Advanced Electric Drive Vehicles*. Boca Raton, FL: CRC Press, Oct. 2014. ISBN: 978-1-4665-9769-3.

[2] F. Genduso, R. Miceli, C. Rando, and G. Galluzzo, "Back emf sensorless-control algorithm for high-dynamic performance pmsm," *Industrial Electronics, IEEE Transactions on*, vol. 57, no. 6, pp. 2092–2100, 2010.

[3] Z. Chen, M. Tomita, S. Doki, and S. Okuma, "An extended electromotive force model for sensorless control of interior permanent-magnet synchronous motors," *Industrial Electronics, IEEE Transactions on*, vol. 50, no. 2, pp. 288–295, 2003.

[4] S. Chi, Z. Zhang, and L. Xu, "Sliding-mode sensorless control of direct-drive pm synchronous motors for washing machine applications," *Industrial Applications, IEEE Transactions on*, vol. 45, no. 2, pp. 582–590, 2009.

[5] A. Khlaief, M. Bendjedia, M. Boussak, and M. Gossa, "A nonlinear observer for high-performance sensorless speed control of ipmsm drive," *Power Electronics, IEEE Transactions on*, vol. 27, no. 6, pp. 3028–3040, 2012.

[6] S. Bolognani, R. Oboe, and M. Zigliotto, "Sensorless full-digital pmsm drive with ekf estimation of speed and rotor position," *Industrial Electronics, IEEE Transactions on*, vol. 46, no. 1, pp. 184–191, 1999.

[7] H. Kim, K.-K. Huh, R. Lorenz, and T. Jahns, "A novel method for initial rotor position estimation for ipm synchronous machine drives," *Industrial Applications, IEEE Transactions on*, vol. 40, no. 5, pp. 1369–1378, 2004.

[8] J. H. Jang, J. I. Ha, M. Ohto, K. Ide, and S. K. Sul, "Analysis of permanent-magnet machine for sensorless control based on high-frequency signal injection," *Industrial Applications, IEEE Transactions on*, vol. 40, no. 6, pp. 1595–1604, 2004.

[9] L. Gong and Z. Zhu, "Robust initial rotor position estimation of permanent-magnet brushless ac machines with carrier-signal-injection-based sensorless control," *Industrial Applications, IEEE Transactions on*, vol. 49, no. 6, pp. 2602–2609, 2013.

[10] S. Nakashima, Y. Inagaki, and I. Miki, "Sensorless initial rotor position estimation of surface permanent-magnet synchronous motor," *Industrial Applications, IEEE Transactions on*, vol. 36, no. 6, pp. 1598–1603, 2000.

[11] M. Boussak, "Implementation and experimental investigation of sensorless speed control with initial rotor position estimation for interior permanent magnet synchronous motor drive," *Power Electronics, IEEE Transactions on*, vol. 20, no. 6, pp. 1413–1422, 2005.

[12] T. Aihara, A. Toba, T. Yanase, A. Mashimo, and K. Endo, "Sensorless torque control of salient-pole synchronous motor at zero-speed operation," *Power Electronics, IEEE Transactions on*, vol. 14, no. 1, pp. 202–208, 1999.

[13] M. Preindl, *Novel Model Predictive Control of a PM Synchronous Motor Drive*. PhD thesis, Univ. of Padua, Dec. 2013.

[14] D. G. Luenberger and Y. Ye, *Linear and Nonlinear Programming*. New York, NY: Springer, Feb. 2008. ISBN: 978-0-387-74502-2.

[15] M. Preindl and S. Bolognani, "Optimal state reference computation with constrained mtpa criterion for pm motor drives," *Power Electronics, IEEE Transactions on*, vol. 30, no. 8, pp. 4525–4535, 2015.